RSC Advances

PAPER

View Article Online
View Journal | View Issue



Cite this: *RSC Adv.*, 2023, **13**, 19607

# Surface modification of graphene with functionalized carbenes and their applications in the sensing of toxic gases: a DFT study†

Sarah Aldulaijan, [a] Afnan M. Ajeebi,[a] Abdesslem Jedidi,[b] Sabri Messaoudi,[cd] Noureddine Raouafi *[e] and Adnene Dhouib *[a]

Graphene and other 2D materials have gained significant attention in the development of gas sensors. In this study, we employed Density Functional Theory (DFT) to investigate the adsorption properties of diazomethanes (**1a–1g**) with various functional groups (R = OH (a), OMe (b), OEt (c), OPr (d), $CF_3$ (e), Ph (f)) on pristine graphene. Furthermore, we explored the adsorption behavior of activated carbenes (**2a–2g**) generated from the decomposition of diazomethanes on graphene, as well as the functionalized graphene derivatives (**3a–3g**) resulting from [2 + 1] cycloaddition reactions between (**2a–2g**) and graphene. The interaction between these functionalized derivatives (**3a–3g**) and toxic gases was also investigated. Our results revealed that carbenes exhibited a stronger affinity for graphene compared to diazomethanes. The adsorption energy of esters (**3b**, **3c**, and **3d**) on graphene decreased relative to compound **3a**, while **3e** exhibited increased adsorption energy due to the electron-withdrawing effect of fluorine atoms. Additionally, the adsorption energy of phenyl and nitrophenyl groups (**3f** and **3g**) decreased due to their π-stacking interaction with graphene. Importantly, all functionalized derivatives (**3a–3g**) demonstrated favorable interactions with gases. Notably, the derivative **3a**, acting as a hydrogen bonding donor, exhibited superior performance. Furthermore, modified graphene derivatives exhibited the highest adsorption energy with $NO_2$ gas, highlighting their potential for selective $NO_2$ sensing applications. These findings contribute to the understanding of gas-sensing mechanisms and the design of novel graphene-based sensor platforms.

Received 17th April 2023
Accepted 17th June 2023

DOI: 10.1039/d3ra02557h

rsc.li/rsc-advances



## 1 Introduction

In recent years, people have become more aware of the harmful effects of toxic gases on their health and the environment.[1] Each toxic gas has its own unique effect, but when different gases are combined, the risks to both human health and the environment are significantly amplified.[2] Moreover, when the presence of a gas goes unnoticed or is not acknowledged by individuals in a particular location, the situation becomes even more hazardous.[3] Gas sensors are used for many purposes, including industrial production,[4] environmental monitoring,[5] and safety.[6] For instance, they are used in aerospace industry[7] and for military applications.[8] Solid-state gas sensors have many advantages, such as their low power requirements,[9] small size,[10] low cost,[11] low detection limits down to parts-per-million (ppm) levels,[12] high sensitivity,[13] thanks to the use of nanostructured materials as sensing elements.[14,15] Graphene and other 2D materials have demonstrated sensing capabilities for a wide range of gases, with both theoretical and experimental studies revealing low power requirements.[16–18] The high sensitivity of graphene to gas concentration changes enabled it to be embedded in sensory devices.[19] This sensitivity can be attributed to two factors: (i) graphene π orbitals interact with the adsorbates residing on top of the substrate *via* van der Waals interactions[20] and (ii) the high surface-to-volume ratio of graphene, which is an advantage feature of all 2D materials.[21] Moreover, graphene has low electronic noise, which makes it an ideal material for detecting gas molecules on its surface.[22] In 2007, we witnessed the first report dealing with the design of the graphene-based gas sensor, which showcased that even the adsorption of a single molecule affects the device resistance due to the charge carrier concentration, which is a direct measure of

[a]*Chemistry Department, College of Science, Imam Abdulrahman Bin Faisal University, P.O. Box 1982, Dammam 31441, Saudi Arabia. E-mail: saaldulaijan@iau.edu.sa; afnanajeebi@hotmail.com; amdhouib@iau.edu.sa*

[b]*Chemistry Department, Faculty of Science, King Abdulaziz University, Jeddah, 21589, Saudi Arabia. E-mail: ajedidi@kau.edu.sa*

[c]*Laboratoire des Matériaux Molécules et Applications, Université Tunis Carthage, IPEST, La Marsa 2070, Tunisia*

[d]*Department of Chemistry, College of Science, Qassim University, Buraidah 51452, Saudi Arabia. E-mail: S.messaoudi@qu.edu.sa*

[e]*Sensors and Biosensors Group, Laboratory of Analytical Chemistry & Electrochemistry (LR99ES15), Faculty of Science, University of Tunis El Manar, 2092 Tunis El Manar, Tunisia. E-mail: noureddine.raouafi@fst.utm.tn*

† Electronic supplementary information (ESI) available. See DOI: https://doi.org/10.1039/d3ra02557h

the device sensitivity.[23] Since then, both theoretical and experimental studies have focused on the adsorption of various gases on graphene such as carbon dioxide and water molecules, oxygen,[24] sulfur dioxide,[25] hydrogen sulfide,[26] carbon monoxide,[27] nitrogen monoxide/dioxide,[28] and ammonia.[29] These studies examined their effects on the electronic properties both experimentally[30–32] and theoretically.[33–35] The target molecules have stronger interaction energies with modified graphene doped with boron and nitrogen,[29] and the charge transfer between the molecules and the modified graphene substrates is also higher.[29,36]

Several experimental[37,38] and theoretical[39–42] studies on graphene functionalization with carbenes have been conducted with the goal of gaining insights into bandgap manipulation and preparing new functional graphene-based nanomaterials with applications in catalysis, electrocatalysis and sensing. The use of chemical reactive radical to achieve the functionalization is thought to have great potential. Using DFT, Petrushenko investigated the [2 + 1]-cycloaddition of dichlorocarbene on graphene sheets. In addition, the carbenes such as $CR_2$ (R = H, F, $CH_3$, CN, $NO_2$, $OCH_3$, CCH, $C_6H_5$) have been shown to chemically adsorb on graphene *via* the same mechanism.[39] Their insertion resulted in an alteration of the graphene substrate inducing a bandgap opening. The findings showed that cycloaddition on the corner or edge positions has no effect on the planar system of graphene, but center functionalization does. As a result, the [2 + 1] cycloaddition of dichlorocarbene could be a promising method for tuning graphene bandgap.[39] More recently, Baachaoui *et al.* studied the effects of the functionalization of graphene sheets by carbenes through the application of different groups of RCOCH, as a R = –$OCH_3$ (**2a**), –OH (**2b**), –ONa (**2c**) and –Ph (**2d**) and investigated their potential for detecting heavy metals. The functionalized materials **2b** and **2c** had greater $Pb^{2+}$ adsorption, which may be explained by an interaction with the graphene adsorbate, implying that they might be utilized to detect and remove $Pb^{2+}$ ions.[40] The same authors also theoretically investigated graphene functionalization with another family of reactive intermediates, *i.e.* nitrenes, for the purpose of sensing of alkylamines (methylamine, dimethylamine, and trimethylamine). The interactions have energies ranging from −0.04 eV to −0.76 eV and differences in the regions of charge gain and depletion between the groups, due to hydrogen bonding, may be seen in the interactions between a short chain of amines and functionalized graphene. Charge variations in the *p*-carboxyperfluorphenylazide (**1b**) system can be studied experimentally.[42] Following these highlighted studies, many studies on the functionalization of pristine graphene using different methods have shown promising results. Recent DFT studies investigated the electronic properties of coronene decorated with silver ($Ag_6$) clusters as a model for silver graphene-based sensors. They observed that the analytes only interact with the carbene part without any involvement of the graphene component in such complexes, the synergistic effect is usually operational.[43–47]

This highlights the significance of further theoretical and experimental investigations into the utilization of functional carbenes for graphene modification and the introduction of novel properties. In order to gain a precise theoretical understanding in this area, our objective is to employ DFT calculations for examining the functionalization of pristine graphene through activated carbenes and their potential for sensing toxic gases.

## 2 Modeling and computational details

The different structures are studied on the Shaheen II HPC from KAUST in Saudi Arabia. Quantum ESPRESSO (v6.5)[48] package was used to perform the *ab initio* calculations. For all the DFT calculations, a van der Waals semiempirical Grimme's DFT-D3 (version 4) correction[49] was applied consistently. The energy cutoffs for the plane-wave functions and the charge density were set at 40.187 Ry and 326.261 Ry, respectively.

The Projector Augmented Wave (PAW) method was employed, utilizing a PAW basis set constructed with a combination of plane waves and localized functions.[50] The Perdew–Burke–Ernzerhof (PBE)[51] is the exchange-correlation functional used in this work for electronic structure calculations as a first principle Generalized Gradient Approximation (GGA) depends on the electron density and its gradient to solve the Kohn–Sham equations. It is recommended, especially, for studies of molecules interacting with surfaces in solid state materials. In previous theoretical studies,[52–56] the GGA-(PBE) method was also successfully used to study graphene systems. The periodic boundary condition was used with a hexagonal and trigonal lattice supercell of 12.34 × 10.68 × 20 $Å^3$ (periodic lengths of the graphene layer in *x*, *y* and *z* directions), which is large enough to completely remove the image interactions. The modeling of the systems was done using the Avogadro (1.2.0) software.[57] The input files were precisely prepared using BURAI software (v 1.32) (**https://github.com/BURAI-team/burai/**). All graphic, atomic, and charge density visualizations were made using VESTA software[58] and the Materials Square online system. The Brillouin zone was sampled using a 3 × 3 × 1 Monkhorst–Pack *K*-point grid during the geometry optimization (structure relaxation), and the orbital energies were expanded using a Gaussian smearing of 0.01 eV. The atomic coordinates of all systems were optimized until the maximum force on ions was less than $1 \times 10^{-3}$ eV $Å^{-1}$.

The adsorption energy or interaction energy, $\Delta E_{ads}$, determined by using eqn (1):

$$\Delta E_{ads} = E_{system} - (E_{substrate} + E_{adsorbate}) \quad (1)$$

The relaxed geometries, corresponding to the minimal energy of the adsorbates, substrates, and (adsorbate/substrate) systems.

The charge density differences were calculated from fragment charge densities according to eqn (2):

$$\Delta\rho = \rho_{system} - (\rho_{subtrate} + \rho_{adsorbate}) \quad (2)$$

The recovery time was calculated from transition state theory according to eqn (3):[59]

$$\tau = \nu^{-1} \times \exp(|\Delta E_{ads}|/k_b T) \quad (3)$$

where, $\nu$: the frequency of bond breaking ($1 \times 10^{12}$ Hz); $\Delta E_{ads}$: the interaction energy, $k_b$: the Boltzmann constant, and $T$: the system temperature.

# 3 Results and discussion

## 3.1 Purpose of the study

The chemical structures of the activated diazomethanes and the corresponding carbenes are shown in Scheme 1a. The reactive intermediates contain low valence electrons in the carbene atom, and that will contribute to chemical reaction with the graphene sheet by reacting with the carbon–carbon double bond *via* [2 + 1] cycloaddition mechanism (Scheme 1b). Thereafter, these functional groups can interact with toxic gases mostly *via* hydrogen bonds (Scheme 1c). We aim to investigate and compare the ability of different functional groups to interact with toxic gases and to determine the main reasons behind it.

The thermodynamic data and geometrical parameters were estimated to study the physical adsorption energy of the reaction intermediates, which are diazomethanes, activated carbenes, and $N_2$, with a graphene supercell ($5 \times 5$ with 50 carbon atoms) in vertical and horizontal positions to find ideal relaxing derivatives and the best position for chemical reactions. The adsorption energy of the chemical reaction [2 + 1]-cycloaddition of functionalizing groups with graphene was calculated. The calculations of the interaction of the modified graphene (**3a–g**) with toxic gases such as $H_2S$, $NH_3$, and $NO_2$ by relaxing the system of derivatives were investigated. To acquire a deeper understanding of the interaction occurring between the modified graphene and the toxic gases, the difference between the charge densities and the Löwdin charges were determined.

## 3.2 Adsorption thermodynamics of diazomethanes and activated carbenes on pristine graphene

### 3.2.1 Physisorption of diazomethane on pristine graphene.

The adsorption energies ($\Delta E_{ads}$) were calculated using eqn (1). Fig. 1S† for the diazomethane and Fig. 1 for the carbenes show the geometric structures of the physisorption and the thermodynamic data, which are summarized in Table 1. It should be emphasized that the adsorption energies depend on the size of the supercell. From previous research, it was noticed that the less favorable $E_{ads}$ in the smaller graphene supercells like $3 \times 3$ or $4 \times 4$, due to surface stress and geometric constraints, brought about the cycloaddition reaction.[42] The $5 \times 5$ graphene supercell, which is a useful compromise between supercell size and adsorbate size, resulting in good interaction energy and saving computational effort, which is affected when using a smaller or larger size supercell.

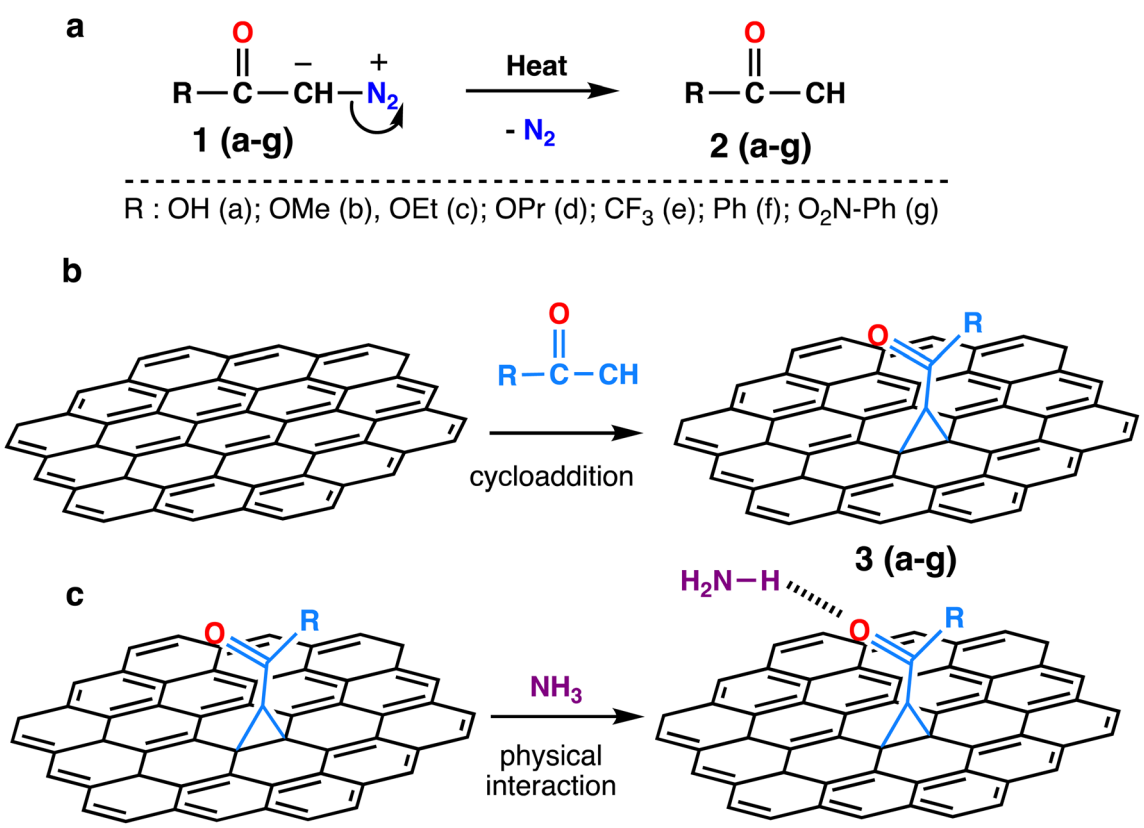


Scheme 1 (a) Starting structures of diazomethanes and the corresponding activated carbenes upon the release of $N_2$ molecule, (b) the chemical reaction of activated carbenes with C=C from the graphene substrate and (c) interaction between cyclopropane-functionalized graphene and ammonia molecule through hydrogen bonding. The carbenes were purposedly represented in cyan for clarity.

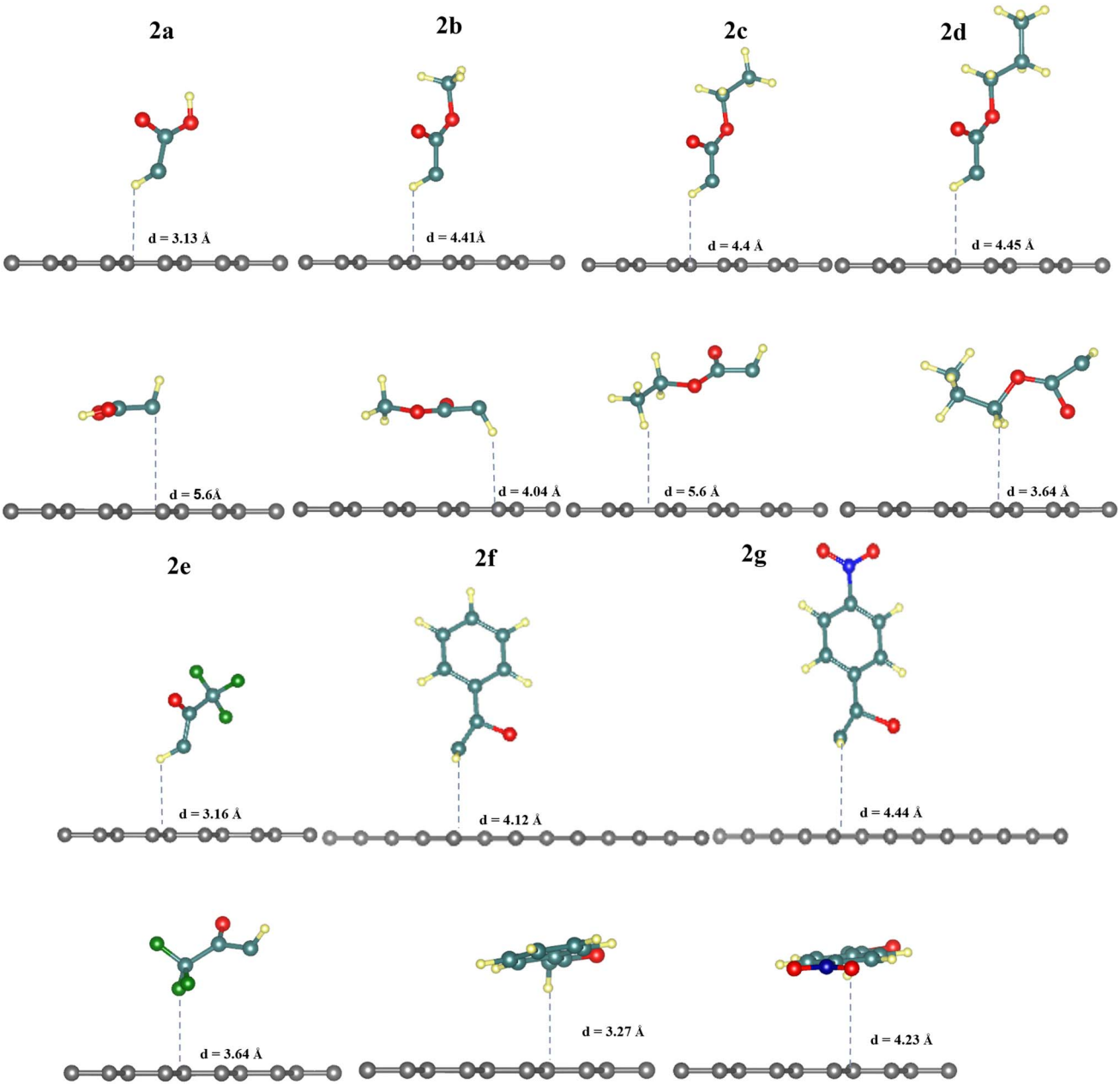


Fig. 1 Relaxed geometries of horizontally and vertically physiosorbed activated carbenes (**2a–g**) on 5 × 5 graphene supercell. Values are for the distances between the closest atom to graphene and the graphene surface depicted from lateral and top views.

The results in Table 1 show that diazomethanes (**1a–g**) do not prefer to interact with graphene 5 × 5 supercell neither in the vertical position (a) nor in the horizontal one (b). Indeed, the interaction energy values are weak (*ca.* −0.20 eV) in 5 × 5 supercell and the distance between diazomethanes and graphene is higher than 3.9 Å.[39,40,42] These characteristics suggest a physisorption process. This also indicates a repulsion between the electronic cloud of graphene and the diazomethanes that contain rich electrons in their dinitrogen atoms, as suggested by Baachaoui *et al.*[40] In addition, $N_2$ has an $\Delta E_{ads}$ is −0.21 eV in all positions studied, including a top, bridge, hollow, and parallel, which is consistent with previous findings.[39,40,42] The adsorption energy value of $N_2$ is equal to or near the diazomethane adsorption values, with no effect for functional groups R, indicating that the diazo is the main part of the adsorption process in the case of diazomethanes.

**3.2.2 Physisorption of activated carbene on pristine graphene.** Activated carbenes (**2a–g**) are formed by the decomposition of diazomethane. They are preferable to interact with the graphene 5 × 5 supercell more than the diazomethanes, as shown by the values of the distances between graphene and the adsorbates in Table 1, which are 3.1 Å to 4.5 Å (Fig. 1). The adsorbates are more likely to occupy a vertical position than a horizontal one. This is due to the electron loss of the nitrogen

Table 1 Adsorption energies of the diazomethanes (**1a–g**) and activated carbenes (**2a–g**) on pristine graphene, and for energies the chemical reaction leading to the formation of (**3a–g**)[a]

| Adsorbates | $\Delta E_{ads}$ (eV) | $d_{ads\text{-}graphene}$ (Å) |
|---|---|---|
| **1a** | −0.21[a] | 4.28 |
| | −0.23[b] | 3.98 |
| **1b** | −0.21[a] | 4.48 |
| | −0.23[b] | 4.68 |
| **1c** | −0.22[a] | 4.34 |
| | −0.22[b] | 4.01 |
| **1d** | −0.23[a] | 4.03 |
| | −0.22[b] | 4.90 |
| **1e** | −0.23[a] | 4.07 |
| | −0.21[b] | 4.64 |
| **1f** | −0.20[a] | 4.43 |
| | −0.24[b] | 3.99 |
| **1g** | −0.21[a] | 4.01 |
| | −0.25[b] | 4.27 |
| $N_2$ | −0.21[c] | 4.18 |
| | −0.21[t] | 3.79 |
| | −0.21[b] | 3.84 |
| | −0.21[h] | 4.19 |
| **2a** | −0.23[a] | 3.56 |
| | −0.24[b] | 5.60 |
| **2b** | −0.22[a] | 4.41 |
| | −0.23[b] | 4.04 |
| **2c** | −0.22[a] | 4.40 |
| | −0.23[b] | 5.60 |
| **2d** | −0.23[a] | 4.45 |
| | −0.25[b] | 4.42 |
| **2e** | −0.24[a] | 3.13 |
| | −0.25[b] | 3.64 |
| **2f** | −0.23[a] | 4.12 |
| | −0.25[b] | 3.27 |
| **2g** | −0.24[a] | 4.44 |
| | −0.28[b] | 4.23 |
| **3a** | −1.67 | 1.56 |
| **3b** | −1.65 | 1.54 |
| **3c** | −1.60 | 1.52 |
| **3d** | −1.64 | 1.54 |
| **3e** | −1.71 | 1.59 |
| **3f** | −1.33 | 1.57 |
| **3g** | −1.39 | 1.58 |

[a] a: vertical, b: horizontal positions. For the nitrogen molecule in c: a top of two carbons in parallel position; t: a top in vertical; b: bridge in vertical; h: hollow positions in vertical; f: new formed C–C bond following the [2 + 1]-cycloaddition chemical reaction.

molecule, and the subsequent formation of electron-deficient carbenes, which increases the attraction between the electronic cloud of graphene and the activated carbenes.

### 3.3 Thermodynamics of the chemical reaction of activated carbenes with pristine graphene

The energies for [2 + 1]-cycloaddition reaction of the carbene functional groups onto the graphene sheet are higher than the physical adsorption energies (Table 1). Because their energies range from −1.33 eV to −1.71 eV, a chemical reaction took place between activated carbene and the graphene surface, which is consistent with literature.[40,42] As shown in Fig. 2, when the carbenes react with the graphene surface they form the cyclopropanes. The newly formed C–C bond lengths are ranging from 1.53 Å to 1.56 Å, which are typical of $sp^3$–$sp^3$ carbon–carbon simple bonds. These distances are longer than the typical C=C bond in graphene which is only of 1.42 Å. Indeed, the hybridization of these carbons changed from $sp^2$ to $sp^3$ following the chemical reaction. These $Csp^3$–$Csp^3$ distance values are similar to those found by Zan in his study of the $R_2C$ (R = H, $CH_3$, Ph, $NO_2$, CN, and Cl) with graphene sheets having an infinite size.[41]

In addition, the cycloadduct **3e** gave slightly higher value of $\Delta E_{ads} = -1.71$ eV compared to other systems with aliphatic side chains (**3a–3d**), with the least long bond of $d^3$ between $C_1$–$C_3$ atoms in the cyclopropane of the react product **3e** with a value of 1.52 Å (see Table S1†), which is a result of electron withdrawing effect by the fluorine atoms in $-CF_3$ group. Moreover, the reaction energies of **3f** and **3g** systems decreased by 10 to 15% (−1.33 eV to −1.39 eV) as an effect of the π-stacking of the aromatic ring on the graphene surface in phenyl and nitrophenyl groups.[40] Thus, the more reactive the carbene is the more reaction energy is. For the electronic withdrawing effects, we can establish the following reactivity of the carbene **3e** > **3a** ≅ **3b** ≅ **3c** > **3f** ≅ **3g**.

As gathered in Table S1,† the cyclopropane internal angles called α and β between the $sp^3$ carbon atoms in graphene sheets and their surrounding neighbors are around 60° and 117°, respectively, which are common in $sp^3$ hybridized carbons of three-membered cycles. The definition of geometrical parameters of the cyclopropane are shown in the Fig. 3.

### 3.4 Detection of gas molecules

Next, we investigated the functionalized graphene derivatives (**3a–g**) as potential nanomaterials for detecting toxic gases such as $H_2S$, $NH_3$ and $NO_2$. From Table 2, one can see that the substrate **3a** gave the highest $\Delta E_{ads}$ results with all gases ranging from −0.25 eV to −0.52 eV, since all of the interactions occurred *via* hydrogen bonds (HB) established between the OH group as HB donor and the lone pairs from the heteroatoms of the gases. Also, the $sp^2$-oxygen in of the carboxylic group, or the H directly bonded to the carbene interact with toxic gases atoms, respectively as HB acceptor or HB donor. The distances are in the range of 1.6 Å to 2.8 Å. For instance, the interaction energy of −0.52 eV found for **3a**/$NH_3$ system is the sum of the contribution from two HB involving the OH group as HB donor and N from $H_3N$ as HB acceptor and a second one linking C=O as HB acceptor to HN from $HN_3$ as HB donor. The first one is stronger since the O–H···N length is 1.63 Å and the second one (C=O···H–N) is weaker since it is 53% longer (2.49 Å).

Furthermore, changing the carboxylic acid ($CO_2H$) by ester groups ($CO_2R$) in (**3b**), (**3c**), and (**3d**), the values of interaction energy decrease and range from −0.05 eV to −0.4 eV with distances of 2.1 Å to 4 Å. This decrease is expected since the interaction involves weak HB and acceptor. In particular for $NH_3$, the remaining interactions involve C=O and H–N, their energy is *ca.* −0.1 eV, which 20% of the energy recorded for the **3a**/$NH_3$ system. This suggests that the O–H···N HB has an energy of *ca.* −0.4 eV. The (**3d**) substrate gives the lowest $\Delta E_{ads}$ compared to

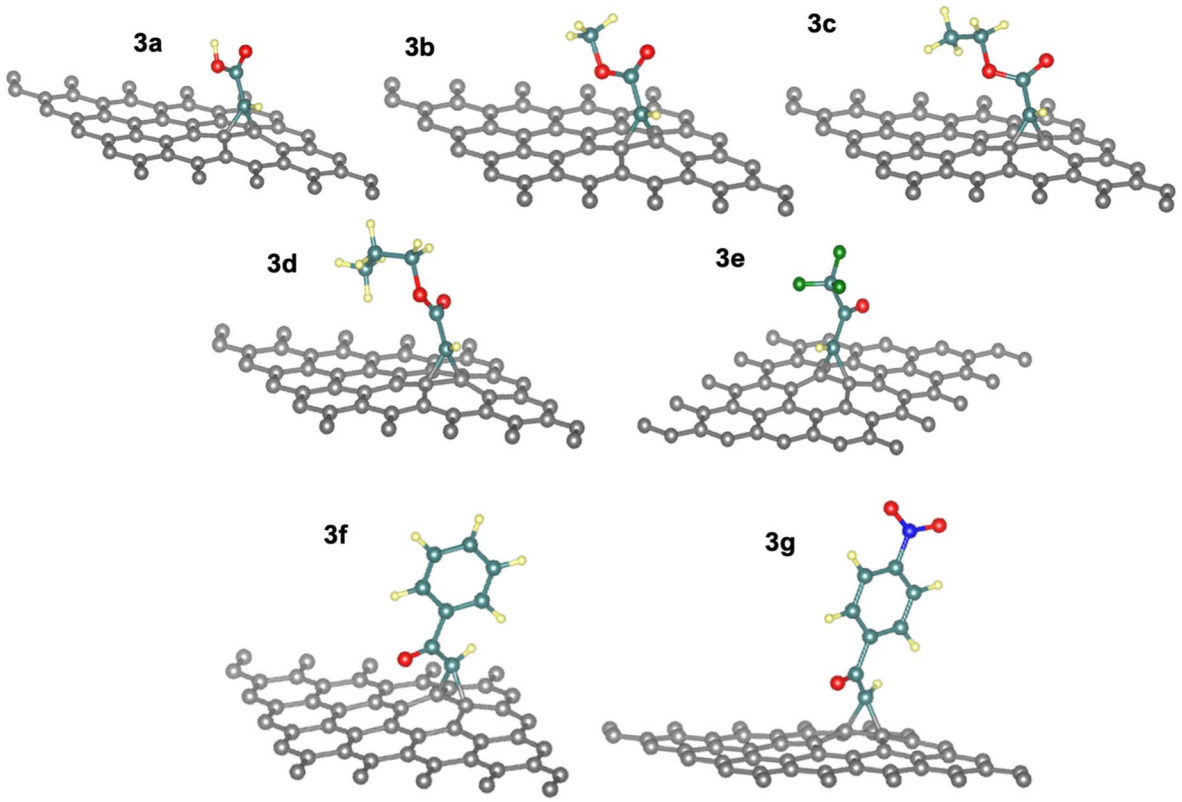


Fig. 2 Optimized geometries of the functionalized graphene nanosheets (**3a–g**).

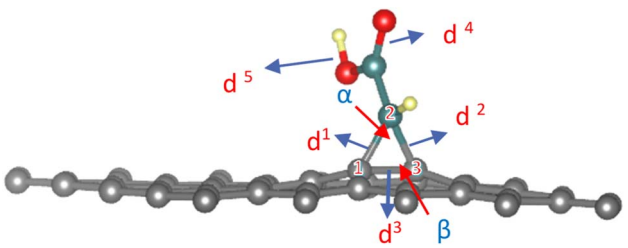


Fig. 3 Geometrical parameters of the cyclopropane definition in modified graphene. Atom labels in the cycloaddition reaction which numbers (1, 2 and 3) and display bond lengths by blue arrows when $d^1$: C1–C2 in (Å); $d^2$: C2–C3 in (Å); $d^3$: C1–C3 in (Å); $d^4$: C=O in (Å); $d^5$: R as a functional group in (Å); h: the highest of C1 and C3 from the level of the graphene main surface (Å), angles are by red arrows when a: angle C1–C2–C3 (°) and b: C1–C3–C2 (°).

other derivatives, because it has a long hydrocarbon chain (OR = $OCH_2CH_2CH_3$), and these steric effects hindered the HB formation with different gases and did not give meaningful results. Finally, the interaction energy of **3e** increased fivefold, by replacement of the $OCH_3$ group with the $OCF_3$ withdrawing group. This effect is observed for all the studied gases, denoting the beneficial effect of introducing electronegative atom on the surface of graphene. The two bearing phenyl graphene systems (**3f** and **3g**) provided lower interaction energies that those with the carboxylic acid group or with the ester groups because the involvement of the C=O in conjugation with the phenyl groups and the graphene network of $sp^2$ carbons.

Particularly, the graphene systems (**3b–3g**) gave the highest $\Delta E_{ads}$ results with $NO_2$ gas compared to other toxic gases. That is due to the interaction of nitrogen dioxide with various functional groups, resulting in the formation of hydrogen bonds CH···O=N in nitrogen dioxide. In the case of **3a**, the interaction implicates the acidic –OH group and the nitrogen from $NO_2$.

### 3.5 Electron density differences and Löwdin partial charges

**3.5.1 Electron density differences.** Using eqn (2), we determined the charge density differences between the individual fragments and the associated **3a**/$NH_3$ and **3d**/$NO_2$ systems (Fig. 4a and c). We can observe that the interactions involve a strong charge variation (*i.e.* blue and yellow colored regions) around the interacting groups while the graphene remains unaffected. The plots correspond to areas of charge depletion (blue) and others of charge gain (yellow). In particular, the charge gain is remarked in between the involved groups (OH and N) and (CH and O). The hydrogens of the ammonia group, of the OH group, oxygen of OH group and the carbon from the C=O groups, all loose parts of the electronic density. Similar observations can be made from the **3d**/$NO_2$ system.

**3.5.2 Löwdin partial charges.** From the final electronic density, we computed the Löwdin partial charges to identify the partial charges on the atoms involved in the interactions (Table 3). In the **3a**/$NH_3$ system after adsorption, the $H^2$ atom ($\delta$ =

Table 2 Interaction energies implicating the substrates (**3a–g**) and $H_2S$, $NH_3$ and $NO_2$, the formed hydrogen bonds and their lengths

| Substrate/gas | | $\Delta E_{ads}$ (eV) | Involved atoms | HB length (Å) | Recovery times (μs) |
|---|---|---|---|---|---|
| **3a** | $H_2S$ | −0.25 | C═O···H–S | 2.23 | <1 |
| | | | O–H···S | 2.30 | |
| | $NH_3$ | −0.52 | O–H···N | 1.63 | 62.3 |
| | | | C═O···H–N | 2.49 | |
| | $NO_2$ | −0.30 | C–H···N | 2.71 | <1 |
| **3b** | $H_2S$ | −0.13 | C═O···H–S | 2.11 | 1.6 |
| | $NH_3$ | −0.10 | C═O···H–N | 2.47 | 4.9 |
| | $NO_2$ | −0.23 | C–H···N | 2.77 | <1 |
| **3c** | $H_2S$ | −0.10 | C═O···H–S | 2.33 | 4.9 |
| | $NH_3$ | −0.11 | C═O···H–N | 2.29 | 7.2 |
| | $NO_2$ | −0.29 | C–H···N | 2.82 | <1 |
| **3d** | $H_2S$ | −0.06 | C–H···S | 3.11 | 1.1 |
| | $NH_3$ | −0.09 | C═O···H–N | 2.25 | 3.3 |
| | $NO_2$ | −0.26 | C–H···N | 2.55 | <1 |
| **3e** | $H_2S$ | −0.10 | C–F···H–S | 2.82 | 295.6 |
| | $NH_3$ | −0.48 | C═O···H–N | 2.83 | 13.1 |
| | $NO_2$ | −0.21 | C–H···N | 3.10 | 46 701.4 |
| **3f** | $H_2S$ | −0.10 | C═O···H–S | 2.19 | <1 |
| | $NH_3$ | −0.09 | C═O···H–N | 2.29 | <1 |
| | $NO_2$ | −0.31 | C–H···O | 2.43 | <1 |
| **3g** | $H_2S$ | −0.07 | N═O···H–S | 2.89 | <1 |
| | $NH_3$ | −0.04 | N═O···H–N | 3.05 | <1 |
| | $NO_2$ | −0.27 | C–H···N | 3.15 | <1 |

+0.37*e*) in the $CO_2H$ group gained an additional electron charge (+0.005*e*), and the $N^1$ ($\delta = -0.75e$) atom in the $NH_3$ gas with loss electron charge (0.083*e*), which demonstrated the interactions between them when the $H^2$ acts as a donor and the $N^1$ as an acceptor in the hydrogen bond. Also, shown the $O^1$ ($\delta = -0.44e$) atom in the $CO_2H$ group with an additional electron charge (0.036*e*) acting as an acceptor to the $H^3$ ($\delta = +0.35e$) atom as a donor in $NH_3$ gas with loss in electron charge (0.022*e*). It can

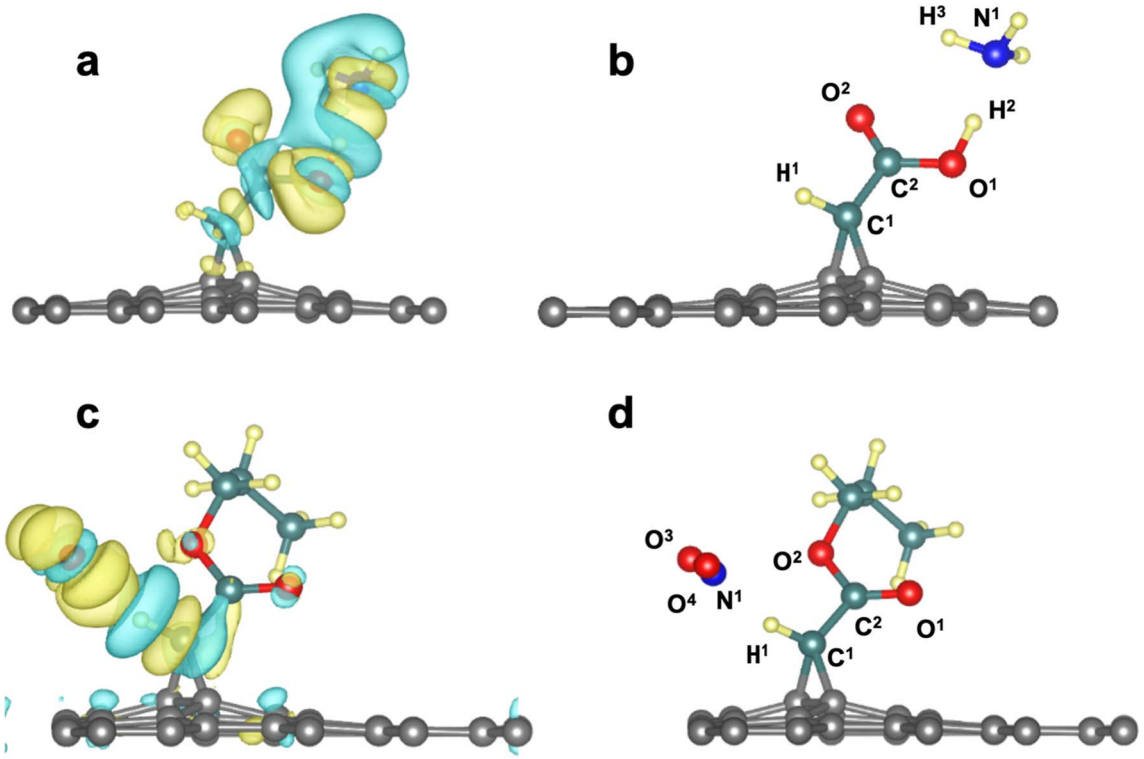


Fig. 4 (a and d) Plot of charge density difference for **3a**/$NH_3$ (**3d**/$NO_2$) showing charge gain (yellow) and charge loss (blue) areas for the atoms involved in the interaction (b and d) labels of the atom of the **3a**/$NH_3$ system reported in Table 3.

Table 3 The Löwdin valence electrons of **3a**/$NH_3$ and **3d**/$NO_2$ and the computed partial (between parentheses) and the percentage of variation. Vertical up and down arrows indicate charge increase or decrease respectively

| Atoms | Valence electrons before interaction (partial charge) | Valence electrons after interaction (partial charge) | Charge variation ($10^2 \times \Delta e/e$) |
|---|---|---|---|
| **3a/$NH_3$** | | | |
| $C^1$ | 4.167 (−0.17) | 4.165 (−0.17) | 0.2 (↓) |
| $C^2$ | 3.417 (+0.58) | 3.425 (+0.58) | 0.8 (↑) |
| $H^1$ | 0.760 (+0.24) | 0.766 (+0.23) | 0.6 (↑) |
| $H^2$ | 0.578 (+0.42) | 0.629 (+0.37) | 5.1 (↑) |
| $O^1$ | 6.399 (−0.40) | 6.435 (−0.44) | 3.6 (↑) |
| $O^2$ | 6.416 (−0.42) | 6.448 (−0.45) | 3.2 (↑) |
| $N^1$ | 5.837 (−0.84) | 5.754 (−0.75) | 8.3 (↓) |
| $H^3$ | 0.673 (+0.33) | 0.651 (+0.35) | 2.2 (↓) |
| **3d/$NO_2$** | | | |
| $C^1$ | 4.164 (−0.16) | 4.159 (−0.16) | 0.5 (↓) |
| $C^2$ | 3.443 (+0.56) | 3.445 (+0.56) | 0.2 (↑) |
| $H^1$ | 0.766 (+0.23) | 0.792 (+0.21) | 2.6 (↑) |
| $O^1$ | 6.392 (−0.39) | 6.391 (−0.39) | 0.1 (↓) |
| $O^2$ | 6.286 (−0.29) | 6.290 (−0.29) | 0.4 (↑) |
| $N^1$ | 4.42 (+0.58) | 4.44 (+0.56) | 0.2 (↑) |
| $O^3$ | 6.241 (−0.24) | 6.290 (−0.29) | 4.9 (↑) |
| $O^4$ | 6.026 (−0.03) | 6.051 (−0.05) | 2.5 (↑) |

be noticed that the closer the atoms got to the interaction region, the clearer the charge variations got, like $O^1$, N1, and $O^2$, and the further away the charge variations decreased, like $C^1$. In the **3d** system after interaction with $NO_2$, the partial charges of $H^1$ atoms closer to the active carbene is ($\delta = +0.21e$) with minor difference in the charge variation of $H^1$ ($\delta^+$) is ($0.002e$), and the partial charge of the $O^4$ is ($\delta = -0.05e$) in the $NO_2$ gases, with additional in the charge variation of $O^4$ ($\delta^-$) is ($0.025e$). These results agree with the adsorption energy values, which are affected by the hydrocarbon chain. It is clear that interactions between them are limited.

### 3.6 Recovery times

Next, we determined the recovery times from the interaction energy at ambient temperature (298 K) using eqn (3) (Table 2). The recovery times range from less 1 μs to 46 701 μs (46.7 ms), when the energy increases from *ca.* −0.10 eV to −0.69 eV. Such short times aren't enough to realize the detection in a real experimental setup because the sensing device cannot hold the gas for times long enough to make the readout.[60] Further increase of the interaction by tuning the acidity of the carboxylic acid by adding electron withdrawing group or change from the carboxylic acid to more acidic sulfonic acid.[61]

## 4 Conclusion

In this work, we firstly investigated the physical adsorption of a series of activated azomethane derivatives and the corresponding substituted carbenes on the surface of pristine graphene. In a second step, we examined the chemical reaction of the reactive intermediates, *i.e.* substituted carbenes, with pristine graphene. The data show clearly that the chemical reaction is favored to the physical adsorption, since the former is higher than the latter. Indeed, the chemical reaction yielded an energy reaction from −1.33 eV to −1.71 eV, while the physical adsorption activated azomethane and carbenes derivatives has an energy of −0.20 eV. The chemical reaction depends on the nature of the adsorbate electronegativity. We further examined the use of (**3a–g**) as substrates for gas sensing. $H_2S$, $NH_3$, and $NO_2$ interact with the substrates *via* hydrogen bonds. The interaction energy ranges from weak (*ca.* −0.10 eV) to medium (*ca.* −0.70 eV), denoting that **3a** and **3d** can be used as substrates for gas sensors since they provide interaction energy lower than −0.50 eV. The interaction can be confirmed by the electron density differences and Löwdin partial charges, since they showed charge gains and losses of the atoms involved in the hydrogen bonds and the partial charges changed by up to 8% from the initial values. Recovery times showed that **3a** and **3d** can be used for sensing after a tuning of their acidity to increase the interaction strengths.

## Conflicts of interest

There are no conflicts to declare.

## Acknowledgements

For computer time, this research (ref. k1495) used the resources of the Supercomputing Laboratory at King Abdullah University of Science & Technology (KAUST) in Thuwal, Saudi Arabia.

## References

1 A. Ghorani-Azam, B. Riahi-Zanjani and M. Balali-Mood, *J. Res. Med. Sci.*, 2016, **21**, 65.
2 A. Siddiqua, J. N. Hahladakis and W. A. K. A. Al-Attiya, *Environ. Sci. Pollut. Res.*, 2022, **29**, 58514–58536.

3 I. Manisalidis, E. Stavropoulou, A. Stavropoulos and E. Bezirtzoglou, *Front. Public Health*, 2020, **8**, DOI: 10.3389/fpubh.2020.00014.
4 R. Bogue, *Sens. Rev.*, 2015, **35**, 133–140.
5 X. Chen, M. Leishman, D. Bagnall and N. Nasiri, *Nanomaterials*, 2021, **11**, 1927.
6 T. Hübert, L. Boon-Brett, V. Palmisano and M. A. Bader, *Int. J. Hydrogen Energy*, 2014, **39**, 20474–20483.
7 S. B, A. John and P. K. Panda, *Sens. Int.*, 2021, **2**, 100085.
8 C. Esteves, E. Ramou, A. R. P. Porteira, A. J. Moura Barbosa and A. C. A. Roque, *Adv. Opt. Mater.*, 2020, **8**, 1902117.
9 G. W. Hunter, S. Akbar, S. Bhansali, M. Daniele, P. D. Erb, K. Johnson, C.-C. Liu, D. Miller, O. Oralkan, P. J. Hesketh, P. Manickam and R. L. vander Wal, *J. Electrochem. Soc.*, 2020, **167**, 037570.
10 Y. Wang, A. Liu, Y. Han and T. Li, *Polym. Int.*, 2020, **69**, 7–17.
11 Y. Wang, A. Liu, Y. Han and T. Li, *Polym. Int.*, 2020, **69**, 7–17.
12 S. Steinhauer, *Chemosensors*, 2021, **9**, 51.
13 Z. Bielecki, T. Stacewicz, J. Smulko and J. Wojtas, *Appl. Sci.*, 2020, **10**, 5111.
14 S. Dhall, B. R. Mehta, A. K. Tyagi and K. Sood, *Sensors*, 2021, **2**, 100116.
15 V. Gargiulo, M. Alfè, L. Giordano and S. Lettieri, *Chemosensors*, 2022, **10**, 290.
16 F. Schedin, A. K. Geim, S. v. Morozov, E. W. Hill, P. Blake, M. I. Katsnelson and K. S. Novoselov, *Nat. Mater.*, 2007, **6**, 652–655.
17 W. Yuan and G. Shi, *J. Mater. Chem. A*, 2013, **1**, 10078.
18 C. Melios, C. E. Giusca, V. Panchal and O. Kazakova, *2D Mater.*, 2018, **5**, 022001.
19 S. Taioli, P. Umari and M. M. de Souza, *Phys. Status Solidi B*, 2009, **246**, 2572–2576.
20 A. Ayatollahi, M. R. Roknabadi, M. Behdani, N. Shahtahmassebi and B. Sanyal, *Phys. E*, 2021, **127**, 114498.
21 N. R. Glavin, C. Muratore and M. Snure, *Oxf. Open Mater. Sci.*, 2020, **1**(1), itaa002.
22 S. Varghese, S. Varghese, S. Swaminathan, K. Singh and V. Mittal, *Electronics*, 2015, **4**, 651–687.
23 F. Schedin, A. K. Geim, S. v. Morozov, E. W. Hill, P. Blake, M. I. Katsnelson and K. S. Novoselov, *Nat. Mater.*, 2007, **6**, 652–655.
24 N. Askari Ardehjani and D. Farmanzadeh, *Adsorption*, 2019, **25**, 661–667.
25 J. Dai and J. Yuan, *J. Phys.: Condens. Matter*, 2010, **22**, 225501.
26 V. E. Comparán Padilla, M. T. Romero de la Cruz, Y. E. Ávila Alvarado, R. García Díaz, C. E. Rodríguez García and G. Hernández Cocoletzi, *J. Mol. Model.*, 2019, **25**, 94.
27 Z. M. Ao, J. Yang, S. Li and Q. Jiang, *Chem. Phys. Lett.*, 2008, **461**, 276–279.
28 J. Dai and J. Yuan, *Chem. Phys.*, 2012, **405**, 161–166.
29 Y.-H. Zhang, Y.-B. Chen, K.-G. Zhou, C.-H. Liu, J. Zeng, H.-L. Zhang and Y. Peng, *Nanotechnology*, 2009, **20**, 185504.
30 A. Ghosh, D. J. Late, L. S. Panchakarla, A. Govindaraj and C. N. R. Rao, *J. Exp. Nanosci.*, 2009, **4**, 313–322.
31 Y. Dan, Y. Lu, N. J. Kybert, Z. Luo and A. T. C. Johnson, *Nano Lett.*, 2009, **9**, 1472–1475.
32 X. Fan, K. Elgammal, A. D. Smith, M. Östling, A. Delin, M. C. Lemme and F. Niklaus, *Carbon*, 2018, **127**, 576–587.
33 T. O. Wehling, K. S. Novoselov, S. v. Morozov, E. E. Vdovin, M. I. Katsnelson, A. K. Geim and A. I. Lichtenstein, *Nano Lett.*, 2008, **8**, 173–177.
34 T. O. Wehling, A. I. Lichtenstein and M. I. Katsnelson, *Appl. Phys. Lett.*, 2008, **93**, 202110.
35 J. Berashevich and T. Chakraborty, *Phys. Rev. B: Condens. Matter Mater. Phys.*, 2009, **80**, 115430.
36 G. Lee, G. Yang, A. Cho, J. W. Han and J. Kim, *Phys. Chem. Chem. Phys.*, 2016, **18**, 14198–14204.
37 W. Yan, Y. Xu and Y. Chen, *J. Nanosci. Nanotechnol.*, 2015, **15**, 2020–2026.
38 T. Sainsbury, M. Passarelli, M. Naftaly, S. Gnaniah, S. J. Spencer and A. J. Pollard, *ACS Appl. Mater. Interfaces*, 2016, **8**, 4870–4877.
39 I. K. Petrushenko, *Monatsh. Chem.*, 2014, **145**, 891–896.
40 S. Baachaoui, S. Aldulaijan, L. Sementa, A. Fortunelli, A. Dhouib and N. Raouafi, *J. Phys. Chem. C*, 2021, **125**, 26418–26428.
41 W. Zan, *Appl. Surf. Sci.*, 2014, **311**, 377–383.
42 S. Baachaoui, S. Aldulaijan, F. Raouafi, R. Besbes, L. Sementa, A. Fortunelli, N. Raouafi and A. Dhouib, *RSC Adv.*, 2021, **11**, 7070–7077.
43 T. Jadoon, T. Mahmood and K. Ayub, *J. Mol. Graphics Modell.*, 2021, **103**, 107824.
44 T. Jadoon, T. Mahmood and K. Ayub, *J. Phys. Chem. Solids*, 2021, **153**, 110028.
45 T. Jadoon, F. Ullah, T. Mahmood and K. Ayub, *Mater. Sci. Semicond. Process.*, 2021, **134**, 106023.
46 T. Jadoon, T. Mahmood and K. Ayub, *J. Mol. Liq.*, 2020, **306**, 112878.
47 T. Jadoon, A. Ahsin, F. Ullah, T. Mahmood and K. Ayub, *J. Mol. Liq.*, 2021, **341**, 117415.
48 P. Giannozzi, O. Andreussi, T. Brumme, O. Bunau, M. Buongiorno Nardelli, M. Calandra, R. Car, C. Cavazzoni, D. Ceresoli, M. Cococcioni, N. Colonna, I. Carnimeo, A. Dal Corso, S. de Gironcoli, P. Delugas, R. A. DiStasio, A. Ferretti, A. Floris, G. Fratesi, G. Fugallo, R. Gebauer, U. Gerstmann, F. Giustino, T. Gorni, J. Jia, M. Kawamura, H.-Y. Ko, A. Kokalj, E. Küçükbenli, M. Lazzeri, M. Marsili, N. Marzari, F. Mauri, N. L. Nguyen, H.-V. Nguyen, A. Otero-de-la-Roza, L. Paulatto, S. Poncé, D. Rocca, R. Sabatini, B. Santra, M. Schlipf, A. P. Seitsonen, A. Smogunov, I. Timrov, T. Thonhauser, P. Umari, N. Vast, X. Wu and S. Baroni, *J. Phys.: Condens. Matter*, 2017, **29**, 465901.
49 M. Dion, H. Rydberg, E. Schröder, D. C. Langreth and B. I. Lundqvist, *Phys. Rev. Lett.*, 2004, **92**, 246401.
50 G. Kresse and D. Joubert, *Phys. Rev. B: Condens. Matter Mater. Phys.*, 1999, **59**, 1758–1775.
51 J. P. Perdew, K. Burke and M. Ernzerhof, *Phys. Rev. Lett.*, 1996, **77**, 3865–3868.
52 W. I. Choi, S.-H. Jhi, K. Kim and Y.-H. Kim, *Phys. Rev. B: Condens. Matter Mater. Phys.*, 2010, **81**, 085441.
53 K. Suggs, D. Reuven and X.-Q. Wang, *J. Phys. Chem. C*, 2011, **115**, 3313–3317.

54 J. Dai and J. Yuan, *Phys. Rev. B: Condens. Matter Mater. Phys.*, 2010, **81**, 165414.
55 X.-G. Xiong, A. Sugiura and T. Yanai, *J. Chem. Theory Comput.*, 2020, **16**, 4883–4898.
56 I. K. Petrushenko, *Monatsh. Chem.*, 2014, **145**, 891–896.
57 M. D. Hanwell, D. E. Curtis, D. C. Lonie, T. Vandermeersch, E. Zurek and G. R. Hutchison, *J. Cheminf.*, 2012, **4**, 17.
58 K. Momma and F. Izumi, *J. Appl. Crystallogr.*, 2011, **44**, 1272–1276.
59 J.-H. Li, J. Wu and Y.-X. Yu, *Appl. Surf. Sci.*, 2021, **546**, 149104.
60 A. Aasi, S. Mehdi Aghaei and B. Panchapakesan, *ACS Omega*, 2021, **6**, 4696–4707.
61 A. Dammak, F. Raouafi, A. Cavanna, P. Rudolf, D. di Caprio, V. Sallet, A. Madouri and J. M. Jancu, *RSC Adv.*, 2022, **12**, 36002–36011.